Comparing Regularized and Non-Regularized Nonlinear Dipole Fit Methods: A Study in a Simulated Sulcus Structure

C.H. Wolters*, R.F. Beckmann^, A. Rienäcker#, and H. Buchner+

Summary: The inverse problem arising from EEG and MEG is largely underdetermined. One strategy to alleviate this problem is the restriction to a limited number of point-like sources, the focal source model. Although the singular value decomposition of the spatio-temporal data gives an estimate of the minimal number of dipoles contributing to the measurement, the exact number is unknown in advance and noise complicates the reconstruction. Classical non-regularized nonlinear dipole fit algorithms do not give an estimate for the correct number because they are not stable with regard to an overestimation of this parameter. Too many sources may only describe noise but can still attain a large magnitude during the inverse procedure and may be indiscernible from the true sources. This paper describes a nonlinear dipole fit reconstruction algorithm with a new regularization approach for the embedded linear problem, automatically controlled by the noise in the data and the condition of the occuring least square problems. The algorithm is stable with regard to source components which "nearly" lie in the kernel of the projection or lead field operator and it thus gives an estimate of the unknown number parameter. EEG simulation studies in a simulated sulcus structure are carried out for an instantaneous dipole model and spatial resolution in the sulcus and stability of the new method are compared with a classical reconstruction algorithm without regularization.

Key words: EEG/MEG; Nonlinear dipole fit; Simulated annealing; Regularization; Truncated singular value decomposition; Finite element method.

Introduction

Source localization of cerebral activity with respect to the individual anatomy is a prominent goal of electro- and magnetoencephalography. The determination of the current distribution inside the brain by means of extracranial field measurements is called the inverse problem. The non-uniqueness of the inverse problem implies that assumptions on the source model, as well as anatomical and physiological a-priori knowledge about the source region and sometimes even results from other techniques like functional magnetic resonance imaging (Menon et al. 1997; Opitz et al. 1999) should be taken into account to obtain a unique solution.

Different source models have been proposed during the last years. One possibility is the restriction to a limited number of dipoles, the focal source model (Scherg and von Cramon 1985; Vaughan 1974). The various spatio-temporal focal source models differ in the manner in which they describe the time dependence of the data. Generally, they are grouped into three classes: the unconstrained dipole model (so-called moving dipole), dipoles with temporally fixed location (rotating dipole) and dipoles with fixed location and fixed orientation (fixed dipole). If only one single time "snapshot" is taken into account, the three classes merge in a spatial dipole model, the so-called instantaneous state dipole model (Wood 1982).

Another proposition is the distributed source model, where the restriction to a limited number of focal sources is abolished. The non-uniqueness of the resulting problem is compensated by the assumption that the dipole strengths should be minimal with regard to a specific norm. Different norms have been proposed, such as the linear L2-norm (Hämäläinen and Ilmoniemi 1994), leading to a smooth current distribution with minimal source energy and the nonlinear L1-norm (Rienäcker et al. 1997; Wagner et al. 1996), which results in a more focal distribution.

* Max-Planck-Institute of Cognitive Neuroscience and Max-Planck-Institute for Mathematics in the Sciences, Leipzig, Germany.

^ Hewlett-Packard GmbH, Böblingen, Germany.

BMW Rolls-Royce GmbH, Dahlewitz, Germany.

+ Department of Neurology, RWTH Aachen, Germany.

Accepted for publication: June 9, 1999.

The authors wish to thank PD. Dr. Helmut Jarausch, Institute for Geometry and Practical Mathematics, RWTH Aachen, Germany for his helpful comments and Prof. Dr. A.D. Friederici and the VW foundation for financial support.

Correspondance and reprint requests should be addressed to Carsten Wolters, Aussenstelle des Max-Planck-Instituts fuer neuropsychologische Forschung, AG Magnetenzephalographie, Muldentalweg 9, 04828 Bennewitz, Germany.

Fax: +49-(0)3425-8875-11

E-mail: wolters@cns.mpg.de

This paper deals with the focal source model. Mosher et al. (1992) showed how a common linear algebraic framework can be formulated for the three spatio-temporal dipole models. One can conclude from this formulation that measured fields depend nonlinearly on dipole location and fixed orientation and linearly on dipole moment strength. Thus, after having chosen the number of sources, nonlinear algorithms should determine their locations (and possibly fixed orientations) and embedded linear methods their moment strength. Another important parameter is the number of active source components, which is normally unknown in advance, but which is required as an input parameter for spatio-temporal dipole modeling. One possibility for the determination of the number parameter was described by Mosher et al. (1992). They proposed to separate the signal and noise subspaces and thus to visually determine the number of source components through the drop in the magnitude of the smallest signal eigenvalue to the greatest noise eigenvalue of the estimated spatial data covariance matrix $\frac{1}{(n-1)}\Phi_{\epsilon}^{me}\left(\Phi_{\epsilon}^{me}\right)^{tr}$ (n: number of samples, m: number of channels, $m \times n$ matrix Φ_{ϵ}^{me}: measured data). This procedure assumes that the signals have a sufficient strength and that they are sufficiently uncorrelated during the time interval. An algorithmic way for the determination of the number parameter is offered by information criteria (Knösche et al. 1998). Under the assumption that the measurements are noise-free and the rank of the projection or lead field operator is maximal (i.e., no source component projects in the data null space), the number of non-zero eigenvalues of the data covariance matrix equals the number of independent source components. Information criteria are based on a statistical concept of separating the space spanned by the principal components of the estimated data covariance matrix into a signal and a noise part.

We will present a "trial and error" strategy to combine the determination of the unknown number parameter with the localization of the sources using a nonlinear dipole fit method with a new regularization approach. The nonlinear dipole parameters will be calculated iteratively by means of simulated annealing (SA) from combinatorial optimization theory (Buchner et al. 1997; Gerson et al. 1994; Haneishi et al. 1994). Compared to the widely used Nelder-Mead simplex algorithm (Nelder and Mead 1965), the annealing procedure is more calculation-intensive, but tries to globally minimize a cost function regardless of the choice of the starting parameters. If the cooling schedule is sufficiently slow, SA has been shown to converge to the global minimum (Geman et al. 1984). The simplex method can become stuck in local minima as shown for brain-stem auditory evoked potentials (Gerson et al. 1994). The linear parameters will then be determined by linear least square methods, yielding a "best" (will be defined) fit between measured and calculated electric potentials. If dipole components are proposed which "numerically" (nearly) project into the data null space, the corresponding lead field matrix becomes ill-conditioned. In combination with noisy data, least square algorithms based on a complete orthogonal factorization or a singular value decomposition of the lead field matrix (see Theory) can yield physiologically unexplainable results for dipole moment strengths, especially when overestimating the number of active sources. This problem can be solved with dipole fit regularization methods like the truncated singular value decomposition (TSVD) (Wolters et al. 1997) or Tikhonov-Phillips regularization (Fuchs et al. 1998). After presenting the theory with regard to the different spatio-temporal dipole models, simulation studies using the instantaneous state dipole model will be carried out to show, that the SA-TSVD is able to reconstruct a reference configuration in the case of noisy EEG data, even when overestimating the number of active sources and is thus able to give an estimate of the unknown number parameter.

A physiological a-priori information about the source region (influence space) is the assumption that the generators must be located on the folded surface of the brain inside the cortex, ignoring white matter and deeper structures such as basal ganglia, brain stem and cerebellum. The apical dendrites of the large pyramid cells in the cortex are considered the generators of the measured fields. If convolutions of the cortical surface are appropriately modelled by the segmentation procedure, another addition is the anatomical information that the generators are perpendicular to this surface (Lorente de No 1938; Nunez 1990). This limitation to normally oriented dipoles is called the normal-constraint. Because a mathematical dipole models an active source region with a certain extent and the resolution of the inverse current reconstruction by means of noisy EEG data is limited, the influence space can be discretized. In the presented simulations with the program CAUCHY (Buchner et al. 1997), we will use a discrete influence space mesh, which properly describes the simulated sulcus surface. Dipoles can only be placed on mesh nodes (influence nodes) and the normal-constraint will be applied.

The inverse algorithm strongly depends on the quality of a forward method. Here, the potential distribution of the observation space is calculated for a known source. Essential for the accuracy is an appropriate model of the volume conductor and of the field propagation. Since the inclusion of the time dependencies is negligible for typical EEG/MEG frequencies below 1 kHz, the field propagation can be described by the quasistatic approximation of Maxwells system of coupled partial differential equations (PDE), leading to a second order elliptic PDE to be

solved for the potential (Plonsey and Heppner 1967). It can be shown, that the solution of this equation in the variational formulation in combination with boundary conditions of Neumann-type and a Dirichlet-point (reference electrode) exists and is unique (Wolters 1997). Thus, the finite element method can be applied to numerically calculate the potential distribution inside the volume conductor (Bertrand et al. 1991; van den Broek et al. 1996; Buchner et al. 1997). This method allows anisotropic and inhomogeneous conductivities (Haueisen et al. 1995; Marin et al. 1998; Pohlmeier et al. 1997).

Since the differential equation is linear, it is possible to set up a so-called influence or lead field matrix **L**. A column of **L** is established by calculating a forward solution at the measurement nodes for a dipole on an influence node with unit strength in one direction. If the physiological a-priori information and the normal-constraint are applied, there is only one possible dipole direction for each influence node and thus every dipole location is represented by only one column in the lead field matrix and one row in the strength matrix **J**. For the unconstrained case, three columns in **L** represent the three orthogonal unit dipoles at a specific location and three rows in the strength matrix **J** correspond to their time series. For an arbitrary dipole source configuration **J**, the resulting electric potentials can then be inexpensively calculated by $\Phi^c = \mathbf{LJ}$.

An important point is the localization of active neuron assemblies within deep and narrow fissures and sulci because two-thirds of the cerebral cortex lie within these structures. An especially difficult case is the reconstruction of oppositely oriented sources if both sulcus walls have regions of neuronal activity.

In the next section, we will present the underlying theory of the focal inverse current reconstruction algorithms SA-COF and SA-TSVD and we will compare the regularization concept of the TSVD with Tikhonov-Phillips regularization. SA-COF and SA-TSVD have been implemented in CAUCHY and EEG simulation studies using the instantaneous state dipole model have been carried out in a four-sphere model with a simulated sulcus structure embedded in the innermost sphere. The goal was the examination of the localization properties, i.e., spatial resolution and stability, of both algorithms in the sulcus.

Theory

The goal of the focal inverse current reconstruction is to find a location tupel q for a chosen number of p dipoles of the influence space and the corresponding $r \times n$ strength matrix $\mathbf{J}_q$ such that

$$H(q) = \left\| \mathbf{L}_q \mathbf{J}_q - \Phi^{me} \right\|_F^2 \stackrel{!}{=} \min$$

where the $m \times r$ matrix $\mathbf{L}_q$ is the overdetermined lead field matrix (thus $m > r$), corresponding to the location tupel q, the $m \times n$ matrix Φ^{me} are the noise-free measurements (EEG/MEG), where m is the number of channels and n the number of samples and $\|\cdot\|_F$ is the Frobenius-norm. Using the normal-contraint, the number r of columns of $\mathbf{L}_q$ and rows of $\mathbf{J}_q$ equals the number p of dipoles, without this constraint it is $r=3p$.

The minimization task can be split into two problems. First, a physiologically and mathematically suitable model should be developed for the shape of the functional graph H. Every evaluation of H for a given location tupel q contains the construction of the corresponding lead field matrix $\mathbf{L}_q$ and the subsequent determination of the direction and strength matrix $\mathbf{J}_q$ with respect to the noise in the measured data Φ_ϵ^{me}.

The second problem is to find the dipole location tupel q which gives a good approximation of the global minimum of H in a feasible calculation time. This was realized with the SA algorithm implemented in CAUCHY.

We will start with the derivation of the theory for a single timepoint $n=1$ since the instantaneous state dipole model was used for the sulcus simulations. Notationally, we use underlines to indicate vectors and boldface for matrices. The measured and noisy data vector will be denoted as $\underline{\Phi}_\epsilon^{me}$, the noise as $\underline{\Delta\Phi}^{me}$ and the noiseless data as $\underline{\Phi}^{me} = \underline{\Phi}_\epsilon^{me} - \underline{\Delta\Phi}^{me}$ and our problem reduces to

$$H(q) = \left\| \mathbf{L}_q \underline{J} - \underline{\Phi}^{me} \right\|_2^2 \stackrel{!}{=} \min. \qquad (1)$$

Assuming that a dipole location tupel q has been proposed by the SA-algorithm, the linear least square problem (equation 1) with noisy data $\underline{\Phi}_\epsilon^{me}$ should then be solved. Without respect to the noise in the data, one possibility to do so is the generalized inverse (Miller 1979) of the lead field matrix

$$\underline{J}_q^+ = \mathbf{L}_q^+ \underline{\Phi}_\epsilon^{me} = \sum_{i=1}^{r} \frac{1}{\varsigma_i} < \underline{\Phi}^{me} + \underline{\Delta\Phi}^{me}, \underline{u}_i > \underline{v}_i \qquad (2)$$

($<\cdot,\cdot>$ denotes the vector scalar product). The generalized inverse is based on a singular value decomposition (SVD) (Appendix A) of $\mathbf{L}_q$. ς_i, the singular values, are automatically arranged by the SVD such that $\varsigma_1 \geq \varsigma_2 \geq \ldots \geq \varsigma_r > 0$ if full rank of $\mathbf{L}_q$ has been assumed. $\underline{v}_i$, the right singular vectors and $\underline{u}_i$, the left singular vectors, are both arranged with increasing spatial frequency. Another possibility to solve equation 1 is the Complete Orthogonal Factorization (COF) of $\mathbf{L}_q$ (Appendix A). This method

can also handle matrices which do not have full effective rank $r_e = r$, which cannot be guaranteed in practical applications. Generally, the COF numerically produces the same results as the generalized inverse and it also suffers from the fact not to account for the data noise. The only goal of both algorithms is to minimize the residual variance to the noisy data.

In practice, $\mathbf{L_q}$ is often ill-posed during the SA-optimization process. This can be measured with the condition number of the lead field matrix $cond_2(\mathbf{L_q}) = \frac{\varsigma_1}{\varsigma_r}$, which can be quite large. Thus, the singular values, ς_i, get very small and the high spatial frequency components of the noise in the data can be extremely amplified (see equation 2). This has an effect on those spatial dipole components, which "numerically" (nearly) lie in the kernel of $\mathbf{L}_q$. It can lead to source configurations, where dipoles with a large strength nearly cancel each other with regard to their surface potential distribution and only explain noise (for both, EEG and MEG inverse problem). Only considering the MEG inverse problem, radial dipoles also numerically lie in the kernel of $\mathbf{L}_q$ and can get a big strength only to explain MEG noise. Both problems especially appear if the number of active sources is overestimated. The problem can be solved with a regularization of the generalized inverse

$$\underline{J}_\gamma = T_\gamma\left(\mathbf{L}_q^+\right)\underline{\Phi}_\epsilon^{me} = \sum_{i=1}^{r} \frac{1}{\varsigma_i} F_\gamma(\varsigma_i) < \underline{\Phi}_\epsilon^{me}, \underline{u}_i > \underline{v}_i,$$

where F_γ is called a filter (Louis 1989). The choice of

$$F_\gamma(\varsigma) = \frac{\varsigma^2}{\varsigma^2 + \gamma^2}$$

leads to a Tikhonov-Phillips regularization, where the high spatial frequency components in the source space, strongly influenced by the noise in the data space, are attenuated and the condition number of the regularized linear least square problem

$$\left\| \mathbf{L}_q^- \underline{J} - \overline{\Phi}_\epsilon^{me} \right\|_2^2 \stackrel{!}{=} \min$$

with

$$\mathbf{L}_q^- = \begin{pmatrix} \mathbf{L_q} \\ \gamma I \end{pmatrix}$$

and

$$\overline{\Phi}_\epsilon^{me} = \begin{pmatrix} \underline{\Phi}_\epsilon^{me} \\ 0 \end{pmatrix}$$

is ameliorated to $cond_2(\mathbf{L}_q^-) = \sqrt{\frac{\varsigma_1^2 + \gamma^2}{\varsigma_r^2 + \gamma^2}}$ (Hämmerlin and Hoffman 1991). This regularization concept for nonlinear dipole fit methods has recently been applied to source localization (Fuchs et al. 1998).

Another way is to choose the filter

$$F_\gamma(\varsigma) = \begin{cases} 1, & \text{if } \varsigma \geq \gamma \\ 0, & \text{if } \varsigma < \gamma \end{cases},$$

leading to a regularization called the Truncated Singular Value Decomposition (TSVD) (Wolters et al. 1997). This algorithm is simply to implement and has the effect of a lowpass filter. The high spatial frequency components of the data, $\varsigma_i < \underline{J}, \underline{v}_i > \underline{u}_i$, are lying below the noise level and as a consequence, the high spatial frequency components in the source space cannot be reconstructed. Using regularization, information will be lost but otherwise the amplification of the high frequency data components would have a more negative effect on the solution, especially in combination with an overestimation of the number of active sources. Like Tikhonov-Phillips regularization, the TSVD ameliorates the condition of the problem.

The proposed algorithm is an iterative procedure. In every step of the optimization, $\mathbf{L_q}$ is changing and thus the condition of the least square problem. Therefore, an automatic determination of the regularization parameter γ is essential. One possibility is provided by the discrepancy principle (Vainikko 1982, 1983) where the so-called *defect d* to the measured data

$$\begin{aligned} d = \left\| \left(I - \mathbf{L_q} T_\gamma\left(\mathbf{L_q}^+\right)\right) \underline{\Phi}_\epsilon^{me} \right\|_2^2 &= \left\| \underline{\Phi}_\epsilon^{me} - \sum_{i=1}^{r} F_\gamma(\varsigma_i) < \underline{\Phi}_\epsilon^{me}, \mathbf{u}_i > \mathbf{u}_i \right\| \\ &= \left\| \underline{\Phi}_\epsilon^{me} \right\|_2^2 - \sum_{i=1}^{r} F_\gamma(\varsigma_i) \left| < \underline{\Phi}_\epsilon^{me}, \mathbf{u}_i > \right|^2 \\ &\stackrel{\text{TSVD}}{=} \left\| \underline{\Phi}_\epsilon^{me} \right\|_2^2 - \sum_{\varsigma_i > \gamma} \left| < \underline{\Phi}_\epsilon^{me}, \mathbf{u}_i > \right|^2 \end{aligned}$$

is not only minimized, but chosen in dependence of the condition number of $\mathbf{L_q}$ and of the noise $\underline{\Delta\Phi}^{me}$ in the data.

Let $\mathbf{C}$ be the $m \times m$ sample noise covariance matrix, determined e.g., from the signal-free pre-stimulus interval of the measurements, averaged over all epochs. This matrix reflects the spatial distribution and correlation of the noise. $\mathbf{C}$ is a symmetric and positive definite matrix, which can be decomposed into $\mathbf{C} = \mathbf{D}\mathbf{D}^{tr}$ by means of a singular value decomposition. If the noise statistics are

known, i.e., if the number of epochs is sufficiently high in order to obtain a good estimate of the noise covariance matrix, the process of data pre-whitening (Knösche et al. 1998) can be used. Thus, we can restrict the theory to spatially uncorrelated noise where **D** is a diagonal weighting matrix. If we consider only one time point and Gaussian distributed and heteroscedastic (different in each channel) noise with zero mean, every channel i should be weighted according to its own noise standard deviation $\epsilon_i = \left|\underline{\Delta\Phi}_i^{me}\right|$ using the diagonal weighting matrix $\mathbf{D}^{-1}$ with entries $1/\epsilon_i$. We thus get the weighted least square problem

$$H^w(q) = \left\|\mathbf{L}_q \underline{J} - \underline{\Phi}_\epsilon^{me}\right\|_{C^{-1}}^2 = \left\|\mathbf{D}^{-1}\left(\mathbf{L}_q \underline{J} - \underline{\Phi}_\epsilon^{me}\right)\right\|_2^2 \stackrel{!}{=} \min,$$

the weighted regularized inverse

$$\underline{J}_\gamma^w = T_\gamma\left(\left(\mathbf{D}^{-1}\mathbf{L}_q\right)^+\right)\mathbf{D}^{-1}\underline{\Phi}_\epsilon^{me} = \sum_{i=1}^{r}\frac{1}{\varsigma_i^w}F_\gamma\left(\varsigma_i^w\right)<\mathbf{D}^{-1}\underline{\Phi}_\epsilon^{me}, \underline{u}_i^w>\underline{v}_i^w,$$

where $\left\{\varsigma_i^w, \underline{u}_i^w, \underline{v}_i^w\right\}$ is the singular system of the weighted lead field matrix $\mathbf{D}^{-1}\mathbf{L}_q$ and the weighted defect

$$d^w = \left\|\left(I - \mathbf{D}^{-1}\mathbf{L}_q T_\gamma\left(\left(\mathbf{D}^{-1}\mathbf{L}_q\right)^+\right)\right)\mathbf{D}^{-1}\underline{\Phi}_\epsilon^{me}\right\|_2^2 = \left\|\mathbf{D}^{-1}\underline{\Phi}_\epsilon^{me}\right\|_2^2 - \sum_{\varsigma_i^w > \gamma}\left|<\mathbf{D}^{-1}\underline{\Phi}_\epsilon^{me}, \underline{u}_i^w>\right|^2.$$

This leads to the following algorithm for the instantaneous state TSVD (n=1, α_i is a scalar):

- Calculate the singular system $\left\{\varsigma_i^w, \underline{u}_i^w, \underline{v}_i^w\right\}$ of the weighted lead field matrix $\mathbf{D}^{-1}\mathbf{L}_q$ by means of a singular value decomposition
- Choose $R > 1$, initialize $\underline{J}_\gamma^w = 0$ and i=0 and calculate $\bar{d} = \left\|\mathbf{D}^{-1}\underline{\Phi}_\epsilon^{me}\right\|_2^2$
- While $\bar{d} > nR^2$:
  - Increase i by 1, calculate $\alpha_i = \left(\underline{u}_i^w\right)^{tr}\mathbf{D}^{-1}\underline{\Phi}_\epsilon^{me}$, $\underline{J}_\gamma^w = \underline{J}_\gamma^w + \frac{1}{\varsigma_i^w}\underline{v}_i^w\alpha_i$ and $\bar{d} = \bar{d} - \alpha_i^{tr}\alpha_i$
- $d^w = \bar{d}$, stop the procedure

T_γ is an order optimal regularization procedure (Louis 1989; Vainikko 1982). The greater the free parameter R is chosen, the stronger the regularization will be. Most of the following simulations in the sulcus structure have been carried out with R=2, but some results show that the choice $R \in [1.1,...,1.5]$ would be more appropriate because of the small number r of source components.

The extension of the SA-TSVD to spatio-temporal modeling (n>1) is straightforward for the moving and for the rotating dipole model. In these cases, $\underline{\alpha}_i$ is the $1 \times n$ vector

$$\underline{\alpha}_i = \left(\underline{u}_i^w\right)^{tr}\mathbf{D}^{-1}\Phi_\epsilon^{me},$$

$\frac{1}{\varsigma_i^w}\underline{v}_i^w\underline{\alpha}_i$ is an $r \times n$ matrix and the euclidian norm should be exchanged for the Frobenius-norm. The SA-TSVD can also simply be applied to the approximate approach of the fixed dipole model, described by Mosher et al. (1992). In this approach, the dipole strengths for each dipole location tupel q are initially calculated under the assumption of rotating orientations. After that, the orientations are fixed by singular value decompositions of the $3 \times n$ submatrices $\mathbf{J}_i$ in $\mathbf{J}_q = (\mathbf{J}_1,...,\mathbf{J}_p)^{tr}$ which describe the strengths in the three unit directions of every dipole. The fixed orientations are defined as the first left singular vectors of the submatrices $\mathbf{J}_i$. The appeal for this approximate approach lies in the reduced computational effort. A computationally more intensive implementation for the fixed dipole model could be the embedding of a projected gradient method or a penalty method for the determination of the two nonlinear orientation parameters into the SA optimization process for the dipole locations and the calculation of the linear dipole strength parameters by means of the TSVD.

Methods

In the following study, the focal inverse current reconstruction methods without (SA-COF) and with regularization (SA-TSVD) are applied to a simulated sulcus structure in order to study their stability when overestimating the number of active sources and the spatial resolution of their reconstruction results in the sulcus. A four layer sphere model with a simulated sulcus embedded in the innermost sphere was constructed (table I), see also (Beckmann et al. 1997). Deeper in the sulcus the walls are parallel with a distance of 6 mm, the opening is described by two opposite hyperbolic functions. The sulcus has a depth of 22 mm and a width of 17 mm. This model was read into the CURRY (Philips Research Laboratories, Research Division Technical Systems, Hamburg, Germany) software-package in order to generate a 3D-

Table I. Parameters of the four layer sphere model with embedded sulcus used for computations.

layer	outer radius (mm)	conductivity (S/m)
1 (brain)	78 (without embedded sulcus)	0.336
2 (liquor)	81 (including the sulcus)	1.0
3 (skull)	90	0.0042
4 (scalp)	96	0.336

tetrahedral finite element mesh in CAUCHY-readable format respecting the segmented four surfaces of the model (figure 1). This led to 97581 tetrahedra and 18213 nodes. 126 electrodes (1 reference electrode at Cz) were distributed regularly over the skin surface in accordance to the 10/10 system (figure 2). The brain surface mesh, appropriately modeling the convolution of the sulcus, was chosen as discrete influence space with 3446 influence nodes (figure 1) and the corresponding lead field matrix was calculated using the anatomical normal-constraint. The calculations were carried out in CAUCHY and visualization of reference sources, generated noisy potential distributions (rereferenced to common average) and inverse source reconstructions was done in CURRY. In the following simulations, reference sources were placed on surface mesh nodes inside the sulcus (figure 3) and of the inner sphere and the potential distribution at the electrode locations was calculated. As a measure for the global field strength, we used the euclidean norm of the calculated electrode potentials (zero potential at Cz)

$$\left\|\underline{\Phi}^c\right\|_2 = \sqrt{\sum_{i=1}^{126}\left(\underline{\Phi}^c\right)_i^2}.$$

Noise was then added and the resulting potential distribution was used to simulate the measurement data for the focal inverse source reconstruction. The noise was assumed to be Gaussian distributed with zero mean and heteroscedastic, thus $\mathbf{D}^{-1}$ being a diagonal weighting matrix. The signal to noise ratio (SNR) was varied for the different simulations. It is defined as

$$SNR = \frac{\sum_{i=1}^{126}\left|\left(\underline{\Phi}_{\epsilon}^{me}\right)_i\right|}{\sum_{i=1}^{126}\epsilon_i}.$$

The focal inverse current reconstruction was then carried out using SA-COF and SA-TSVD with a varying number of dipoles. At first, the activity was limited to one sulcus wall, then both sulcus walls were active and in the last simulation we used separated reference sources.

Results

Each of the deeper sources 1*l*, 1*r*, 2*l*, 2*r*, 3*l*, 3*r* and 4*l*, 4*r* with normalized strength (100*nAm*) generated a global field strength $\left\|\underline{\Phi}^c\right\|_2$ of 25 up to 30 μV. Surface-near dipoles have a much greater effect on the electrode potentials, 5*l* and 5*r* of about $\left\|\underline{\Phi}^c\right\|_2$ =71 μV and A*l* and A*r* of about $\left\|\underline{\Phi}^c\right\|_2 = 83\,\mu V$.

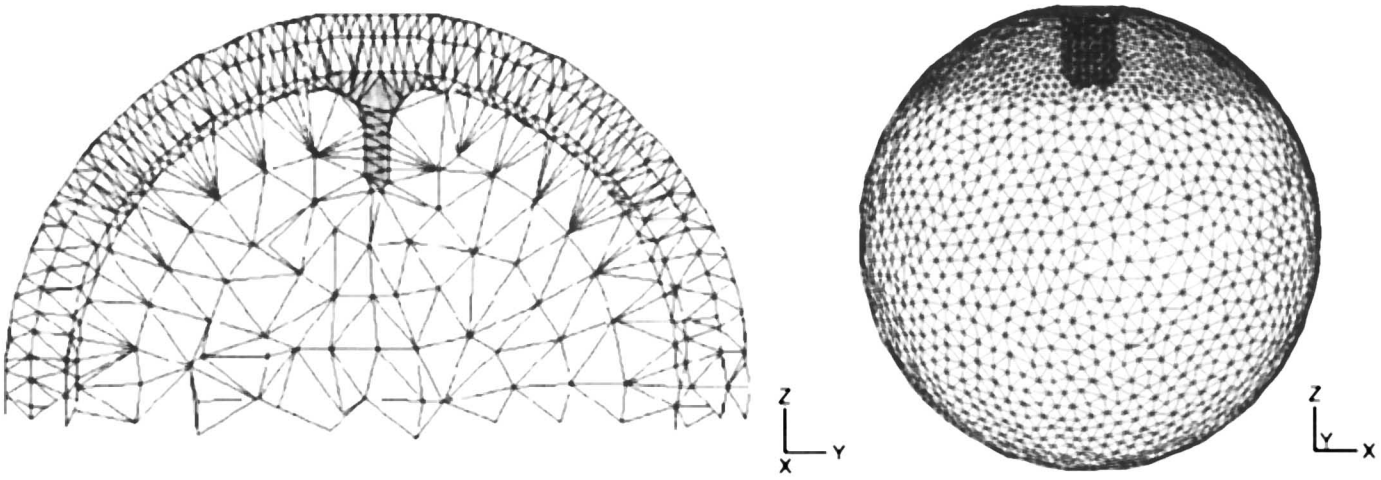

Figure 1. Tetrahedra mesh of the four layer sphere model with embedded sulcus structure. A cross-section through the finite element mesh (left) and the influence space mesh, used for simulations (right).

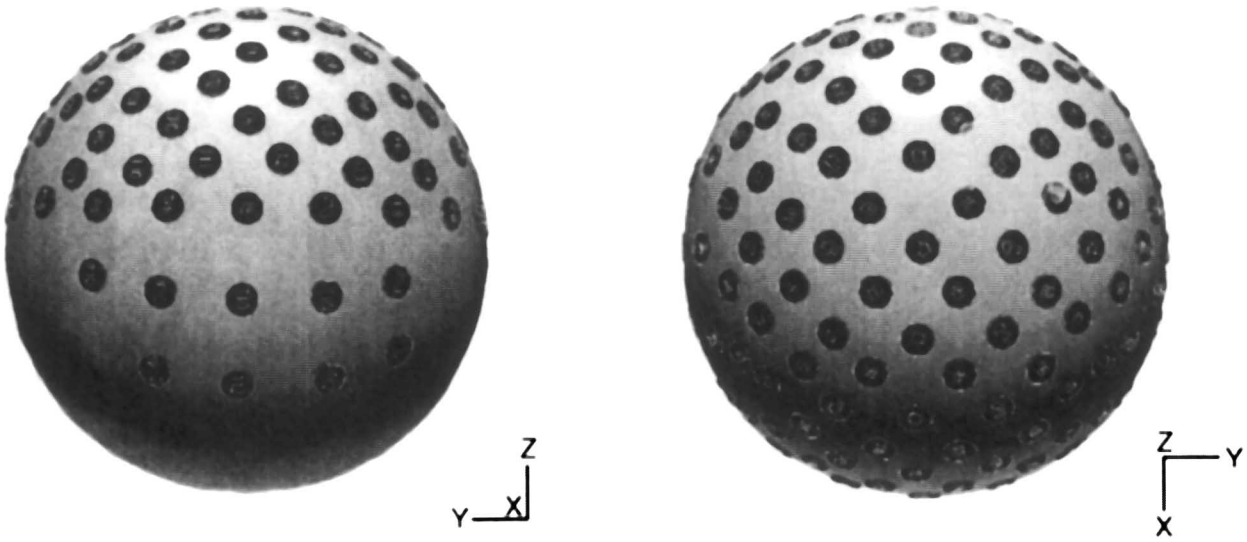

Figure 2. Right view (left) and top view (right) on the electrode positions on the outer sphere surface.

Activity on one sulcus wall

Simulation 1

Six reference dipoles (100*nAm*) were placed in the model (figure 4, top left), one at the sulcus position 5*l* and five at the bottom of the inner sphere only to simulate biological noise (global field strength of the noise dipoles $\|\underline{\Phi}^c\|_2 \approx 4\,\mu V$).

In CAUCHY, forward results are stored with a precision of five digits. When carrying out a focal inverse source reconstruction SA-COF for six dipoles, using the stored potential values, the noise dipoles already could not be reconstructed in contrast to the sulcus source. Five dipoles on the bottom of the inner sphere were found with locations, differing slightly from the locations of the reference noise sources.

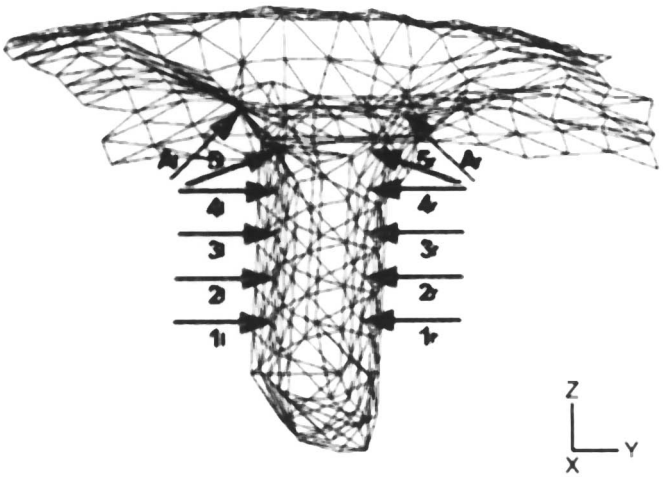

Figure 3. Reference dipole positions on the sulcus walls.

Gaussian distributed noise with $SNR = 17.9$ was then added to the reference potentials. The noisy potential distribution rereferenced to common average is shown in figure 4 (top right). The goal of the inverse search cannot be the reconstruction of the noise dipoles. It should be rather ensured that the left sulcus activity, lying above the noise level, can be emphasized in the result. Therefore, a single dipole model is appropriate and both algorithms, SA-COF and SA-TSVD, yielded the right location 5*l* with an appropriate strength. In practice, the number of active sources is unknown. If for example two dipoles are underlying the measured potentials, the search for one source would not be a good model. In contrast to that, if the number of active sources is overestimated, a desirable result would be the reconstruction of the real sources and the neglect of the remaining ones by assigning small values of strength to them.

SA-COF and SA-TSVD were then carried out with six dipoles. The result is shown in figure 4 (bottom). The defect d of the calculated potentials to the noisy data without regularization is 11 $(\mu V)^2$, with regularization it is 16.4 $(\mu V)^2$. Thus, despite being a better approximation to the measured data, the SA-COF is not stable. The activity in the sulcus was reconstructed (dipole 5*l* with a strength of 91*nAm*), but stays behind a stronger activity of the remaining and only noise-explaining dipoles (strongest dipole 374*nAm*). The regularization method focusses on the sulcus activity and avoids that the remaining defect to the data is explained by strong dipoles, which cancel each other with regard to their potential

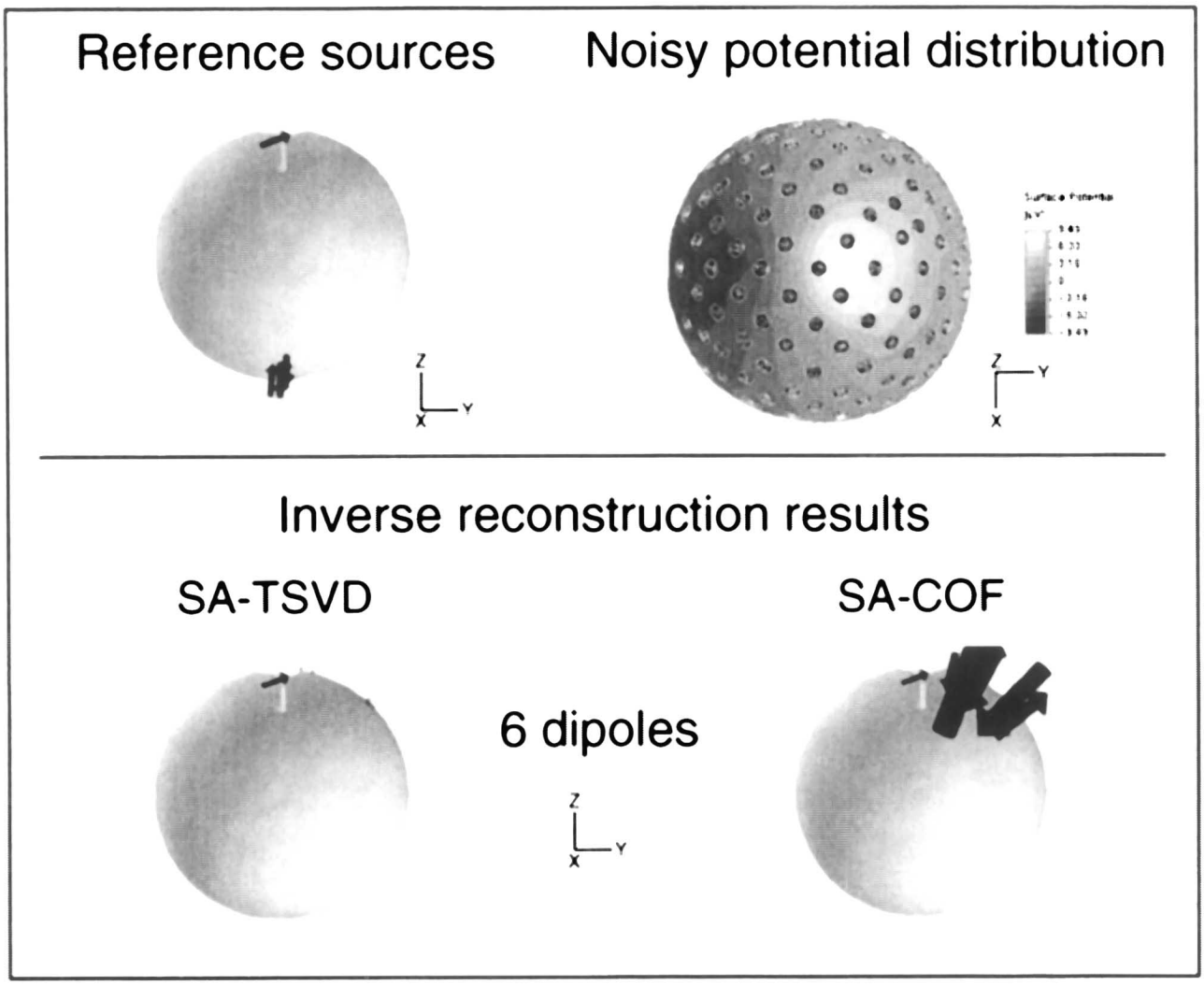

Figure 4. Activity on one sulcus wall: Simulation 1: Reference dipole configuration (top, left), the simulated noisy potential distribution on the outer sphere surface rereferenced to common average (top, right) and the reconstruction results of the SA-TSVD (bottom, left) and SA-COF (bottom, right) when searching for 6 dipoles.

distribution or sources which have a small influence on the potential distribution, like deep sources (EEG and MEG) or radial sources (MEG). Fixing the dipole locations of the SA-COF result and considering the regularized solution of the resulting least square problem, the defect is about 19.6 $(\mu V)^2$. The first right singular vector $\underline{v}_1$ emphasizes the sulcus node 5*l* and already after the first term of the generalized inverse, the defect drops off below the noise level and the discrepancy principle takes effect.

Simulation 2

Six dipoles were placed on the left sulcus wall at the positions 1*l* (100*nAm*), 2*l* (110*nAm*), 3*l* (130*nAm*), 4l (110*nAm*), 5*l* (100*nAm*) and *Al* (100*nAm*) (figure 5, top left). Altogether, this led to a reference potential distribution of $\left\|\underline{\Phi}^c\right\|_2 = 195\,\mu V$. Low Gaussian distributed noise with a *SNR* = 75.3 was then added to these potentials. The noisy potential distribution rereferenced to common average is shown in figure 5 (top right). When fixing the reference dipole locations, figure 5 (middle) shows the solutions of the corresponding least square problem with the TSVD and with the COF (ten times reduced dipole strength). The condition number of the corresponding lead field matrix $\mathbf{L_q}$ is 1960. Thus the least square problem is ill-conditioned and without regularization, the high frequency components of the noise are extremely amplified in the solution. Because the dipole distribution is assumed to be smooth for neighboring sources (like for the current density source model), the

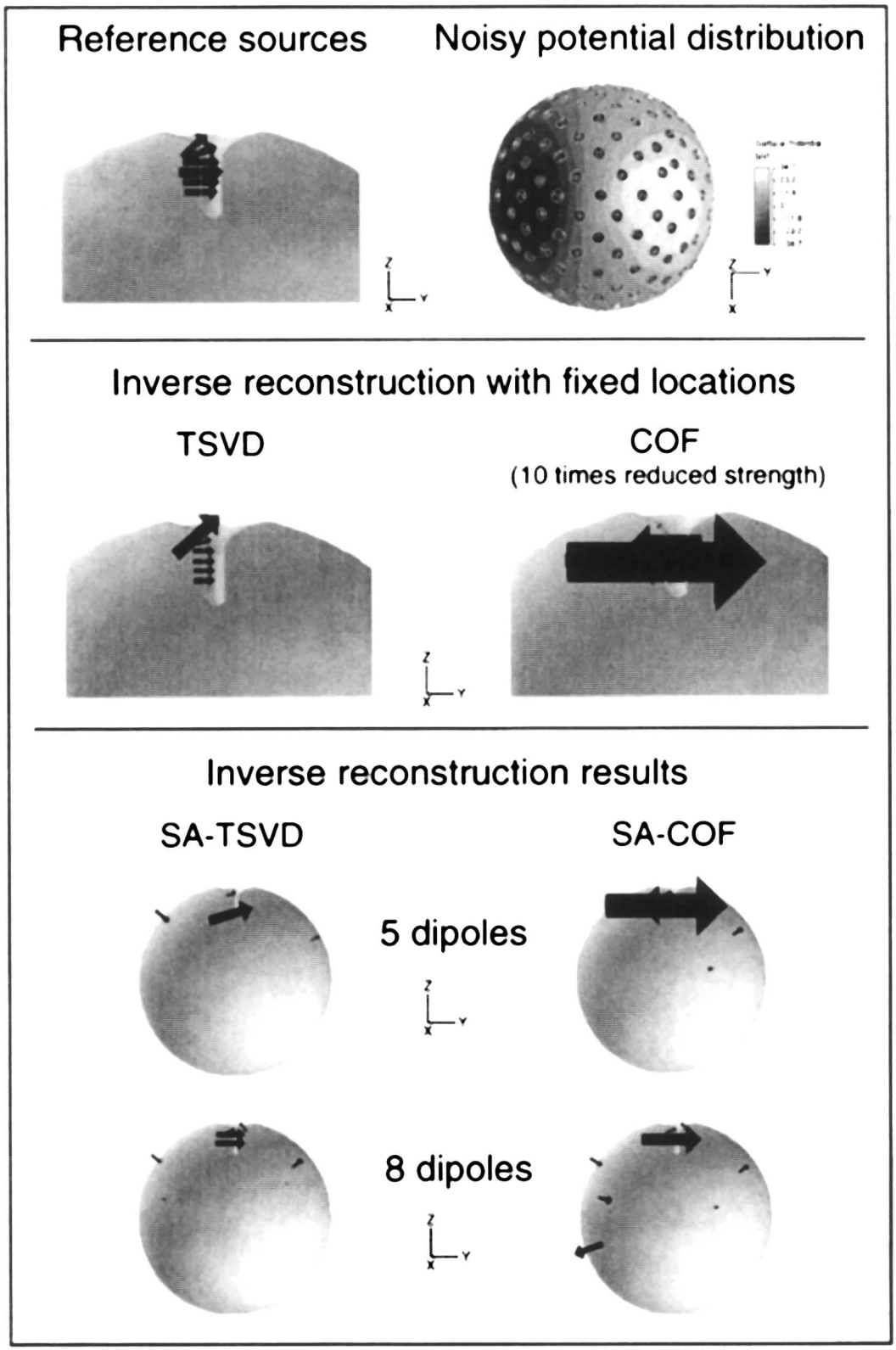

Figure 5. Activity on one sulcus wall: Simulation 2: Reference dipole configuration (top, left), the simulated noisy potential distribution on the outer sphere surface rereferenced to common average (top, right), the solution of the least square problem using the reference dipole locations with TSVD (middle, left) and with COF (ten times reduced dipole strength) (middle, right) and the reconstruction results of SA-TSVD (bottom, left) and SA-COF (bottom, right) when searching for 5 and 8 dipoles.

regularization is a justified and necessary model for noisy data. During the simulated annealing process, high condition numbers often appear for separated dipole locations. In this case, the model of regularization cannot be justified by the smoothness property of the dipole distribution and high frequencies in the source space can be quite meaningful. Here, the regularization can be seen as a method to ameliorate the condition of the problem. The high frequency components in the data space are lying below the noise level and thus, high frequencies in the source space cannot be reconstructed.

SA-COF and SA-TSVD were carried out with five dipoles (figure 5, bottom). The result of the SA-COF has a defect of only $d = 25.8\ (\mu V)^2$, but is not stable with regard to the sulcus wall. The data is explained by a strong dipole on the left wall (990*nAm*), weakened by a source on the right wall with opposite direction (490*nAm*). The problem is ill-posed and the high frequency component had a strong influence in the result. The solution of the regularization method has a defect of 27.9 $(\mu V)^2$ and is stable concerning the sulcus wall but it should be mentioned that a result with dipoles on both sulcus walls with the same direction can not be precluded. In the following, eight dipoles were searched for (figure 5, bottom). Both algorithms show the main activity on the left sulcus wall. The spatial resolution of the SA-TSVD is better. One part of the noise-flawed reference potential distribution can be explained by three dipoles, one at sulcus position *Ar*, a second on the left side of the sphere surface with an orientation of approximately 45 degrees and a third at the same height on the right side of the sphere surface. With the SA-COF, a second part of the noise is explained by a deep and strong source, lying at the bottom left of the sphere surface, the method is getting unstable.

Activity on both sulcus walls

Six opposing dipoles were placed on the left and right sulcus wall at the positions 1*l* (100*nAm*), 2*l* (110*nAm*), 3*l* (100*nAm*), 1*r* (100*nAm*) 2*r* (120*nAm*) and 3*r* (100*nAm*) (figure 6, top left). Because of the eliminating effect the potential had an euclidian norm of only $\left\|\underline{\Phi}^c\right\|_2 =$ 36.8 μV. Noise yielding a *SNR* of 11.35 was added to these potentials (figure 6, top right, rereferenced to common average) and the inverse reconstruction for 6 and 7 dipoles was carried out with both algorithms (figure 6, bottom). When searching for 7 dipoles, the SA-COF could reconstruct the sulcus activity with a defect of $d = 4.7$ $(\mu V)^2$, while the SA-TSVD tended to a "zero-solution" and a defect of $d = 5.3\ (\mu V)^2$ was left to the data. The regularization with $R = 2.0$ was too careful with regard to the noise and to the high spatial frequencies of the reference source configuration.

Separated activity

More than one active source region normally contributes to integrative processes of the brain and the locations of the involved sources can be quite separated. In the last simulation, three dipoles were placed in the sulcus structure, one on the left sulcus wall at position 1*l* (200*nAm*) and two further sources on the surface of the inner sphere (100*nAm*) (figure 7, top left). The reference potential had an euclidian norm of $\left\|\underline{\Phi}^c\right\|_2 = 71\ \mu V$. Using these noiseless data, the SA-COF could exactly reconstruct the reference source configuration when searching for three dipoles. Noise with *SNR* = 16.6 was added to these potentials (figure 7, top right). When searching for three dipoles, the SA-COF, just like the SA-TSVD with the regularization parameter $R \in [1.1,...,1.5]$ could reconstruct the reference configuration with only a small localization error. The error for the SA-TSVD was more significant when choosing R=2.0. In this case, the regularization is too careful and the loss of information too large for the small dimension of the source space.

The inverse reconstruction for 5 and 8 dipoles indicates the stabilizing effect of the regularization (figure 7, bottom).

Discussion and Conclusions

We have presented a new regularization approach for nonlinear dipole fit algorithms and we have carried out simulations using the instantaneous state dipole model (single time slice of data, typically at the peak of the observed EEG response). The focal inverse source reconstruction algorithm simulated annealing in combination with the regularization method TSVD shows good properties to determine "sure" sources. Dipoles which have a measurable effect on the data, will be reconstructed and do not sink into insignificance beside stronger and physiologically unexplainable sources which only explain noise and nearly cancel each other (EEG and MEG) or deep sources (EEG and MEG) or radial sources (MEG). The derived algorithm accounts for heteroscedastic noise in the data, especially in combination with bad condition numbers of the least square problems, occuring during the inverse search. It especially seems to be more stable regarding an overestimation of the number of active dipoles when compared with non-regularized nonlinear dipole fit algorithms like it is the SA-COF. In combination with the singular value decomposition of the spatio-temporal data, giving an estimate for the minimal number, the exact number of dipoles can better be enclosed. This can be seen as a "trial and error" strategy of determining the number of sources, compared with the statistical concept of the information criteria, working in the data space (Knösche

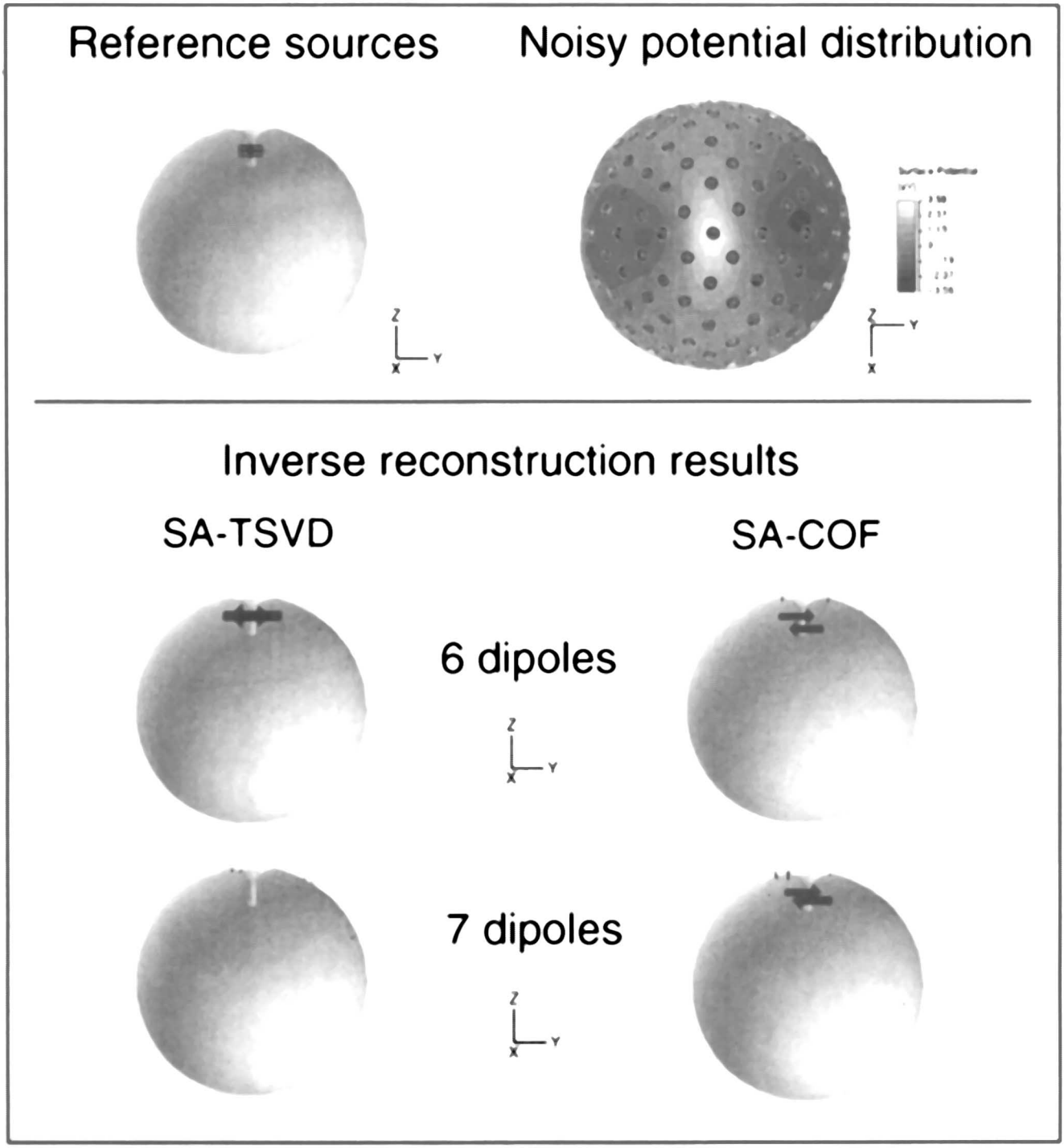

Figure 6. Activity on both sulcus walls: Reference dipole configuration (top, left), the simulated noisy potential distribution on the outer sphere surface rereferenced to common average (top, right) and the reconstruction results of SA-TSVD (bottom, left) and SA-COF (bottom, right) when searching for 6 and 7 dipoles.

et al. 1998) or the method based on the SVD of the measurement data, proposed by (Mosher et al. 1992). The strength of the regularization, controlled by the parameter R, should not be chosen too large, because it is proportional to the loss of information and because the dimension of the source space is small. The choice $R \in [1.1,...,1.5]$ for the TSVD showed the best performance during our simulations.

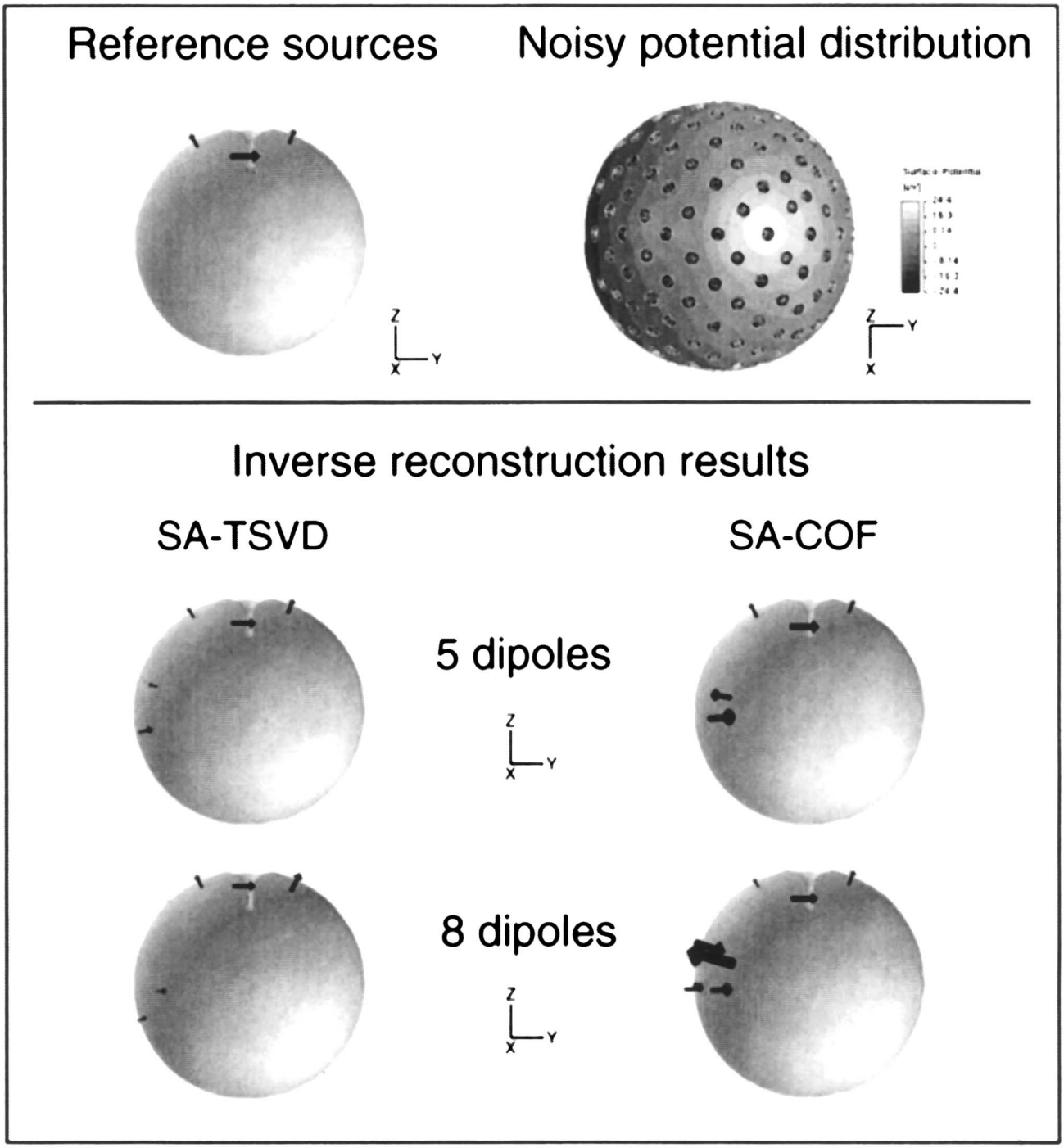

Figure 7. Separated activity: Reference dipole configuration (top, left), the simulated noisy potential distribution on the outer sphere surface rereferenced to common average (top, right) and the reconstruction results of SA-TSVD (bottom, left) and SA-COF (bottom, right) when searching for 5 and 8 dipoles.

With regard to spatio-temporal modeling, as we have shown, the SA-TSVD can simply be extended to the moving dipole model (unconstrained location and orientation), to the rotating dipole model (fixed location, unconstrained orientation) and to the fixed dipole model approach, proposed by Mosher et al. (1992). When embedding a further nonlinear algorithm to determine the two fixed orientation parameters during the SA process for the location parameters, e.g., projected gradient methods or penalty methods, the regularization concept of the

SA-TSVD can also be applied to the fixed dipole model (fixed locations and fixed orientations). Nevertheless, it should be mentioned that this procedure will be quite computationally time-consuming.

The presented regularization concept can be of special importance, if dipole locations are already known (a-priori information, e.g., functional magnetic resonance imaging constrained dipole fits) whose corresponding lead field matrix is ill-posed.

In our sulcus simulations with the focal source model, the influence space was discretized with 3446 influence nodes. According to the anatomical constraint and because of the appropriate modeling of the sulcus-convolution by the influence space mesh, the normal-constraint could be applied so that for every influence node only the strength parameter had to be determined. If reference activity is restricted to one sulcus wall and noise complicates the reconstruction, high spatial frequency inverse source configurations like dipoles on both sulcus walls having opposite directions can have a strong influence in the result of non-regularized dipole fit methods like the SA-COF, especially when overestimating the number of dipoles. The regularized SA-TSVD is more stable with regard to the sulcus wall, but it cannot be precluded that small dipoles on the opposite sulcus wall with the same dipole moment direction are added to explain the data. This is the principle of the shadow (Wang 1994), who examined the MNLS inverse (minimum norm least squares, distributed source model) in a simulated sulcus structure.

If both sulcus walls are active and the dipoles nearly cancel each other with regard to their surface potential distribution, the regularization method tends to the "zero-solution" proportional to the size of the regularization parameter R, to the noise in the data and to the chosen number of dipoles. The loss of information with a strong regularization of $R = 2.0$ and the choice of seven active dipoles during simulation was too strong to reveal the underlying sulcus activity. A choice of $R \in [1.1,...,1.5]$ or fewer dipoles was more adequate and even in the case of noisy data, the activity on both sulcus walls was reconstructed.

Appendix A

The following methods, based on different decompositions of the overdetermined $m \times r$ $(m > r)$ lead field matrix $\mathbf{L_q}$ for solving the linear least square problem

$$H(q) = \left\| \mathbf{L_q J} - \Phi_{\epsilon}^{me} \right\|_F^2$$

have been implemented in CAUCHY:

QR-Decomposition

If $\mathbf{L_q}$ has full rank r, it can be decomposed into an orthogonal $m \times m$ matrix $\mathbf{Q}$ ($\mathbf{Q}^{tr}\mathbf{Q}=\mathbf{I}$) and an $m \times r$ matrix

$$\mathbf{R} = \begin{pmatrix} \mathbf{R_1} \\ \mathbf{0} \end{pmatrix}$$

with a right upper triangular $r \times r$ matrix $\mathbf{R_1}$ (see e.g., Werner 1991). The coefficient matrix of the reduced system has the same condition as the lead field matrix

$$cond_2\,(\mathbf{L_q}) = cond_2\,(\mathbf{QR}) = cond_2\,(\mathbf{R}).$$

The application of $\mathbf{Q}^{tr}$ to the measured (noisy) data Φ_{ϵ}^{me} yields

$$\mathbf{Q}^{tr}\Phi_{\epsilon}^{me} = \begin{pmatrix} \Phi_{\epsilon 1}^{me} \\ \Phi_{\epsilon 2}^{me} \end{pmatrix}$$

with an $r \times n$ matrix $\Phi_{\epsilon 1}^{me}$ and an $(m\text{-}r) \times n$ matrix $\Phi_{\epsilon 2}^{me}$. Because orthogonal transformations preserve the Frobenius-norm, the linear least square problem

$$H(q) = \left\| \mathbf{Q}^{tr}\mathbf{L_q J} - \mathbf{Q}^{tr}\Phi_{\epsilon}^{me} \right\|_F^2 = \left\| \mathbf{R_1 J} - \Phi_{\epsilon 1}^{me} \right\|_F^2 + \left\| \Phi_{\epsilon 2}^{me} \right\|_F^2$$

can be solved by back-substitution $\mathbf{R_1 J} = \Phi_{\epsilon 1}^{me}$.

To numerically calculate the QR-decomposition, we used the method of Householder (see e.g., Werner 1991), implemented in subroutine DGEQPF (LAPACK 1992). The left orthogonal matrix is represented as a product of elementary Householder rotation matrices $\mathbf{H}(i) = \mathbf{I} - \tau_i \underline{x}_i \underline{x}_i^{tr}$ with a scalar τ_i and an $m \times 1$ vector $\underline{x}_i$, i.e.,

$$\mathbf{Q} = \mathbf{H}\,(1) \cdot \ldots \cdot \mathbf{H}\,(m).$$

Complete Orthogonal Factorization (COF)

Generally it cannot be guaranteed, that the overdetermined $m \times r$ $(m > r)$ lead field matrix $\mathbf{L_q}$ has full effective rank $r_e = r$. This is why a QR-decomposition with column pivoting

$$\mathbf{L}_q\mathbf{P} = \mathbf{Q}\begin{pmatrix} \mathbf{R}_{11} & \mathbf{R}_{12} \\ \mathbf{0} & \mathbf{R}_{22} \end{pmatrix}$$

is calculated in a first step of the COF, where the $r_e \times r_e$ matrix $\mathbf{R}_{11}$ is defined as the largest leading submatrix whose estimated condition number is less than $1/R_{cond}$

with a small constant R_{cond}. In our simulations, we defined $R_{cond} = 0.3 \cdot 10^{-7}$. Thus, the order of $\mathbf{R}_{11}$ is the effective rank r_e of $\mathbf{L}_q$. In a second step of the COF, the $(m\text{-}r_e) \times (r\text{-}r_e)$ matrix $\mathbf{R}_{22}$ is considered to be neglegible and the $r_e \times (r\text{-}r_e)$ matrix $\mathbf{R}_{12}$ is annihilated by the $r \times r$ orthogonal right Householder rotation matrix $\mathbf{Z}$:

$$[\mathbf{R}_{11} \quad \mathbf{R}_{12}] = [\mathbf{R}_1 \quad \mathbf{0}]\mathbf{Z}$$

If we write

$$\mathbf{Q} = \left[\mathbf{Q}_{r_e} \quad \mathbf{Q}_{m-r_e}\right],$$

where $\mathbf{Q}_i$ contains the first i columns of $\mathbf{Q}$ and

$$\mathbf{Z} = \begin{bmatrix} \mathbf{Z}_{r_e} \\ \mathbf{Z}_{r-r_e} \end{bmatrix}$$

where $\mathbf{Z}_i$ contains the first i rows of $\mathbf{Z}$, we arrive at the COF of the lead field matrix

$$\mathbf{L}_q\mathbf{P} = \left[\mathbf{Q}_{r_e} \quad \mathbf{Q}_{m-r_e}\right]\begin{pmatrix} \mathbf{R}_1 & \mathbf{0} \\ \mathbf{0} & \mathbf{0} \end{pmatrix}\begin{bmatrix} \mathbf{Z}_{r_e} \\ \mathbf{Z}_{r-r_e} \end{bmatrix}.$$

The linear least square problem $H(q)$ can then be solved by

$$\mathbf{J}_q = \mathbf{P}\mathbf{Z}_{r_e}^{tr}\mathbf{R}_1^{-1}\mathbf{Q}_{r_e}^{tr}\Phi_\epsilon^{me}.$$

For our simulations, we used subroutine DGELSX (LAPACK 1992).

Singular Value Decomposition (SVD) and Generalized Inverse

A third strategy is based on the well-known singular value decomposition (SVD) of the lead field matrix

$$\mathbf{L}_q = \mathbf{U}\mathbf{S}\mathbf{V}^{tr} = (\underline{u}_1, \ldots, \underline{u}_m)\begin{pmatrix} \Sigma \\ \mathbf{0} \end{pmatrix}(\underline{v}_1, \ldots, \underline{v}_r)^{tr}$$

with the orthogonal $m \times m$ matrix $\mathbf{U}$, the $m \times r$ matrix $\mathbf{S}$ with $\Sigma = diag(\varsigma_1, \ldots \varsigma_r)$ and the orthogonal $r \times r$ matrix $\mathbf{V}$ (see e.g., Werner 1991). For our simulations, we used subroutine DGESVD (LAPACK 1992). It can be shown, that ς_i^2 are the eigenvalues and $\underline{u}_i$ the eigenvectors of $\mathbf{L}_q\mathbf{L}_q^{tr}$ and ς_i^2 the eigenvalues and $\underline{v}_i$ the eigenvectors of $\mathbf{L}_q^{tr}\mathbf{L}_q$. Furthermore, it is

$$\mathbf{L}_q\underline{v}_i = \varsigma_i\underline{u}_i \qquad i = 1, \ldots, r, \tag{3}$$

and

$$\begin{aligned} \underline{u}_i^{tr}\mathbf{L}_q &= \varsigma_i\underline{v}_i^{tr}, \qquad i = 1, \ldots, r, \\ \underline{u}_i^{tr}\mathbf{L}_q &= \underline{0}^{tr}, \qquad i = r+1, \ldots, m. \end{aligned} \tag{4}$$

Thus, the space spanned by $\{\underline{u}_1, \ldots, \underline{u}_r\}$ is called the *column space* and *span* $\{\underline{u}_{r+1}, \ldots, \underline{u}_m\}$ is the so-called *left null space* of $\mathbf{L}_q$. Let $\mathbf{U}_r$ be the $m \times r$ matrix $\mathbf{U}_r = (\underline{u}_1, \ldots, \underline{u}_r)$. Without respect to the noise in the data, the least square problem can be solved by means of the generalized inverse of the lead field matrix, in matrix form

$$\begin{aligned} \mathbf{L}_q^+\underline{\Phi}_\epsilon^{me} &= \left(\mathbf{L}_q^{tr}\mathbf{L}_q\right)^{-1}\mathbf{L}_q^{tr}\underline{\Phi}_\epsilon^{me} = \mathbf{V}\mathbf{S}^+\mathbf{U}^{tr}\underline{\Phi}_\epsilon^{me} \\ &= (\underline{v}_1, \ldots, \underline{v}_r)\left(\Sigma^{-1} \quad \mathbf{0}\right)(\underline{u}_1, \ldots, \underline{u}_m)^{tr}\underline{\Phi}_\epsilon^{me}. \end{aligned}$$

(see also equation 2). Non-regularized nonlinear dipole fit methods use this generalized inverse to solve the linear least square problems embedded in the nonlinear optimization process.

The matrix $\mathbf{P}_L = \mathbf{L}_q\mathbf{L}_q^+$ projects data $\underline{\Phi}$ onto the column space of $\mathbf{L}_q$

$$\mathbf{P}_L\underline{\Phi} = \mathbf{L}_q\mathbf{L}_q^+\underline{\Phi} \overset{(2)}{=} \mathbf{L}_q\sum_{i=1}^{r}\frac{1}{\varsigma_i} < \underline{\Phi}, \underline{u}_i > \underline{v}_i \overset{(3)}{=} \sum_{i=1}^{r} < \underline{\Phi}, \underline{u}_i > \underline{u}_i = \mathbf{U}_r\mathbf{U}_r^{tr}\underline{\Phi}.$$

Mosher et al. (1992) derived an efficient form of calculating $H(q)$, which is based on an SVD of the data matrix $\Phi_\epsilon^{me} = \mathbf{U}_\Phi\mathbf{S}_\Phi\mathbf{V}_\Phi^{tr}$:

$$\begin{aligned} H(q) &= \left\|\Phi_\epsilon^{me} - \mathbf{L}_q\left(\mathbf{L}_q^+\Phi_\epsilon^{me}\right)\right\|_F^2 = \left\|\Phi_\epsilon^{me}\right\|_F^2 - \left\|\mathbf{P}_L\Phi_\epsilon^{me}\right\|_F^2 \\ &= \left\|\mathbf{U}_\Phi\mathbf{S}_\Phi\mathbf{V}_\Phi^{tr}\right\|_F^2 - \left\|\mathbf{U}_r\mathbf{U}_r^{tr}\mathbf{U}_\Phi\mathbf{S}_\Phi\mathbf{V}_\Phi^{tr}\right\|_F^2 = \left\|\mathbf{S}_\Phi\right\|_F^2 - \left\|\mathbf{U}_r^{tr}\mathbf{U}_\Phi\mathbf{S}_\Phi\right\|_F^2 \end{aligned}$$

Orthogonal matrices were dropped in the derivation since they preserve the Frobenius-norm. When using SVD-versions of the lead field matrix, in which only the left singular vectors $\mathbf{U}_r$ are iteratively calculated and when r is small relative to m, this procedure of calculating $H(q)$ will outperform methods based on noniterative QR decompositions, leading to the same result.

References

Beckmann, R., Buchner, H. and Knoll, G. Inverse localization of neuronal activity on opposite walls of a simulated sulcus. In: H. Witte, U. Zwiener, B. Schack and A. Doering (Eds.), Quantitative and Topological EEG and MEG Analysis, Druckhaus Mayer Verlag GmbH Jena-Erlangen, 1997: 484-486.

Bertrand, O., Thévenet, M. and Perrin, F. 3D finite element method in brain electrical activity studies. In: J. Nenonen, H.M. Rajala and T. Katila (Eds.), Biomagnetic Localization and 3D Modelling, Report Department of Technical Physics, Helsinki University, 1991: 154-171.

Buchner, H., Knoll, G., Fuchs, M., Rienäcker, A., Beckmann, R., Wagner, M., Silny, J. and Pesch, J. Inverse localization of electric dipole current sources in finite element models of the human head. Electroencephalogr. and Clin. Neurophysiol., 1997, 102: 267-278.

Fuchs, M., Wagner, M., Wischmann, H.A., Köhler, T., Theißen, A., Drenckhahn, R. and Buchner, H. Improving source reconstructions by combining bioelectric and biomagnetic data, Electroencephalogr. and Clin. Neurophysiol., 1998, 107: 93-111.

Geman, S. and Geman, D. Stochastic relaxation, Gibbs distribution, and the Bayesian restoration of images. IEEE Trans. Pattern Anal. Mach. Intell., 1984, 6: 721-741.

Gerson, J., Cardenas, V.A. and Fein, G. Equivalent dipole parameter estimation using simulated annealing. Electroencephalogr. and Clin. Neurophysiol., 1994, 92: 161-168.

Hämäläinen, M.S. and Ilmoniemi, R.J. Interpreting magnetic fields of the brain: minimum norm estimates, Med. Biol. Eng. Comp., 1994, 32: 35-42.

Hämmerlin, G. and Hoffmann, K.-H. Numerische Mathematik. Springer-Verlag, 2 edition, 1991.

Haneishi, H., Ohyama, N., Sekihara, K. and Honda, T. Multiple current dipole estimation using simulated annealing, IEEE Transactions on Biomedical Engineering, 1994, 41: 1004-1009.

Haueisen, J., Ramon, C., Czapski, P. and Eiselt, M. On the influence of volume currents and extended sources on neuromagnetic fields: A simulation study. Annals of Biomedical Engineering, 1995, 23: 728-739.

Knösche, T.R., Berends, E.M., Jagers, H.R.A. and Peters, M.J. Determining the number of independent sources of the EEG. A simulation study on information criteria. Brain Topography,1998, 11(2): 111-124.

LAPACK, Linear Algebra PACKage User's Guide, SIAM, 1992.

Lorente de No, R. Cerebral cortex: architecture, intracortical connections, motor projections, In: J.F. Fulton, (Ed.), Physiology of the Nervous System, Ch.15. University Press, Oxford, London, 1938.

Louis, A.K. Inverse und schlecht gestellte Probleme. Teubner-Verlag, 1989.

Marin, G., Guerin, C., Baillet, S., Garnero, L. and Meunier G. Influence of skull anisotropy for the forward and inverse problem in EEG: simulation studies using the FEM on realistic head models,Human Brain Mapping, 1998, 6: 250-269.

Menon, V., Ford, J.M., Lim, K.O., Glover, G.H. and Pfefferbaum, A. Combined event-related fMRI and EEG evidence for temporal-parietal cortex activation during target detection, Neuroreport, 1997, 8: 3029-3037.

Miller, K. Least squares methods for ill-posed problems with a prescribed bound. SIAM Journal of Math. Analysis, 1979, 1: 52-74.

Mosher, J.C., Lewis, P.S. and Leahy, R.M. Multiple dipole modeling and localization from spatio-temporal MEG data. IEEE Transactions on Biomedical Engineering, 1992, 39 (6): 541-557.

Nelder, J.A. and Mead, R. A simplex method for function minimization. Comp. J., 1965, 7: 308-313.

Nunez, P.L. Localization of brain activity with electroencephalography. In: S. Sato (Ed.), Magnetoencephalography, Raven Press, New York, 1990: 39-65.

Opitz, B., Mecklinger, A., von Cramon, D.Y. and Kruggel, F. Combining electrophysiological and hemodynamic measures of the auditory oddball. Psychophysiology, 1999, 36: 142-147.

Plonsey, R. and Heppner, D. Considerations on quasi-stationarity in electrophysiological systems. Bull. math. Biophys., 1967, 29: 657-664.

Pohlmeier, R., Buchner, H. and Knoll, G. The influence of skull-conductivity misspecification on inverse source localization in realistically shaped finite element head models. Brain Topography, 1997, 9(3): 157-162.

Rienäcker, A., Buchner, H. and Knoll, G. Comparison of regularized inverse EEG analyses in finite element models of the individual anatomy. In: H. Witte, U. Zwiener, B. Schack and A. Doering (Eds.), Quantitative and Topological EEG and MEG Analysis, Druckhaus Mayer Verlag GmbH Jena-Erlangen, 1997: 459-463.

Scherg, M. and von Cramon, D. Two bilateral sources of the late AEP as identified by a spatio-temporal dipole model. Electroencephalogr. and Clin. Neurophysiol., 1985, 62: 32-44.

Vainikko, G.M. The discrepancy principle for a class of regularization methods. USSR Computational Mathematics and Mathematical Physics, 1982, 22(3): 1-19.

Vainikko, G.M. The critical level of discrepancy in regularization methods. USSR Computational Mathematics and Mathematical Physics, 1983, 23(6): 1-9.

van den Broek, S.P., Zhou, H. and Peters, M.J. Computation of neuromagnetic fields using finite element method and biot savart law. Med. Biol. Eng. Comput., 1996, 34: 21-26.

Vaughan, Jr., H.G. The analysis of scalp-recorded brain potentials. In: R.F. Thompson and M.M. Patterson (Eds.), Bioelectric Recording Techniques. Part B. Academic Press, New York, 1974, 158-207.

Wagner, M., Fuchs, M., Wischmann, H.-A., Drenckhahn, R. and Köhler, Th. Current density reconstructions using the L1-norm. In: Biomag96, Proc. of the 10th Int. Conf. of Biomagnetism; Santa Fe, 1996: 158-207.

Wang, J.-Z. MNLS inverse discriminates between neuronal activity on opposite walls of a simulated sulcus of the brain. IEEE Transactions on Biomedical Engineering, 1994, 41(5): 470-479.

Werner, J. Numerische Mathematik 1. Vieweg, 1991.

Wolters, C. Direkte Methoden zur Berechnung dipolinduzierter elektrischer und magnetischer Felder und inverse Strategien zur Quellokalisation im Gehirn. Diplomarbeit

in Mathematik mit Nebenfach Medizin, Institut fur Geometrie und Praktische Mathematik, RWTH Aachen, 1997.

Wolters, C., Rienäcker, A., Beckmann, R., Jarausch, H., Buchner, H., Grebe, R. and Louis, A.K. Stable inverse current reconstruction in real anatomy using combinatorial optimization techniques combined with regularization methods. In: H. Witte, U. Zwiener, B. Schack and A. Doering (Eds.), Quantitative and Topological EEG and MEG Analysis, Druckhaus Mayer Verlag GmbH Jena-Erlangen, 1997: 487-490.

Wood, C.C. Application of dipole localization methods to source identification of human evoked potentials. Ann. New York Acad. Sci., 1982, 388: 139-155.